BOEING SCIENTIFIC RESEARCH LABORATORIES DOCUMENT NAS 7-489

BOEING

SCIENTIFIC RESEARCH LABORATORIES

CONTRACT NAS 7-489

Stress Corrosion Cracking of Titanium Alloys: Electrochemical Kinetics in Aqueous Solutions and SCC in Molten Salts

T. R. Beck, W. H. Smyrl

Quarterly Progress Report No. 16

for Period of

April 1, through June 30, 1970

and Summarizing work done from

January 1, through June 30, 1970

FACILITY FORM 602

N71 70013 (ACCESSION NUMBER) (THRU)

64 (PAGES) None (CODE)

CR-111624 (NASA CR OR TMX OR AD NUMBER) (CATEGORY)

DEC 1970 RECEIVED NASA STI FACILITY INPUT BRANCH

SOLID STATE PHYSICS LABORATORY JUNE 1970

CONTRACT NAS 7-489

Stress Corrosion Cracking of Titanium Alloys: Electrochemical Kinetics in Aqueous Solutions and SCC in Molten Salts

Quarterly Progress Report No. 16

for Period of

April 1, through June 30, 1970

and Summarizing work done from

January 1, through June 30, 1970

Prepared by

T. R. Beck, and W. H. Smyrl

Solid State Physics Laboratory

Boeing Scientific Research Laboratories

Seattle, Washington 98124

TABLE OF CONTENTS

		Page
1.0	SUMMARY	i
2.0	INTRODUCTION	ii
3.0	TECHNICAL DISCUSSION	1
	3.1 Electrochemical Kinetics	1
	3.2 SCC in Molten Salts	19
4.0	CONCLUSIONS	40
5.0	FUTURE WORK	41
6.0	REFERENCES	42
7.0	APPENDIX	44
	I. What determines i_2 at edge of patches	44
	II. Equation for calculation of $C^{\frac{1}{2}}$	47
	III. Modified equation to calculate values of $C^{\frac{1}{2}}$	50
	IV. Theory for slope of log $C^{\frac{1}{2}}$ vs ϕ	55

1.0 SUMMARY

Further experiments and analyses of electrochemical kinetics of new titanium surfaces and of SCC in molten salts were conducted. New titanium surfaces did not passivate in aqueous HF nor in methanol - HCl solutions. That titanium stress corrodes in methanol-HCl and not aqueous HF indicates that passivation by oxide per se is not an essential criterion for SCC. Model relations for rate of oxide patch growth on titanium in aqueous solutions were derived. Analysis of hydrogen ion mass transport in molten salts indicated that the hydrogen mechanism is unlikely in this case. Experimental evidence for anodic dissolution of titanium in a propagating crack in a molten salt was observed.

2.0 INTRODUCTION

This report describes part of a study of stress corrosion cracking of titanium alloys initiated in July 1965 (1) and continued under NASA sponsorship beginning July, 1966 (2). This is the sixteenth Quarterly Report in the series (3, 4, 5, 6, 7, 8, 9, 10, 11, 12, 13, 14, 15, 16, 17) and covers the six-month period of January 1, through June 30, 1970. A short letter report (17) described work in progress in the period of January 1, through March 31, but did not present detailed results.

The present Quarterly Report describes some additional experiments and theory on electrochemical kinetics of newly generated titanium surfaces and some further SCC experiments in molten salts and analysis of data.

A considerable amount of time and effort was devoted during the past two quarters to writing chapters on stress corrosion cracking of titanium in collaboration with the ARPA SCC program. These chapters will appear in a book on SCC issued by ARPA. A number of assorted experiments on SCC of titanium were conducted during this time to fill in obvious gaps in information. Results of these experiments by themselves did not tell a coherent enough story and thus were not written up separately for this Quarterly Report. The above chapters will be made available as a BSRL document.

3.0 TECHNICAL DISCUSSION

3.1 Electrochemical Kinetics

Some kinetics experiments were conducted in which the output from the potentiostat was sent to the BSRL computer to compile and print out. A comparison of data compiled by the computer and from an oscilloscope photograph of the same run is given in Fig. 1. The data have been improved in accuracy and extended to about an order of magnitude in current by use of the computer but further work needs to be done to decrease the noise level and prevent the oscillations occurring at the low currents. The more accurate data should allow better testing of kinetic models.

3.1.1 Experiments in HF and Methanol-HCl

The HF and Methanol-HCl tests were made to determine the kinetic behavior of fresh titanium surfaces in presumably non-passivating environments. Results of a run in 3M HF at -500 mv are shown in Fig. 2. (A Teflon Luggin capillary and salt bridge were used.) The current rose but did not decay with time as in 3 M HCl. A second trace taken about one second after the break gave the same plateau current, indicating that passivation did not occur. The current density could not be calculated accurately because the reaction occurred on an extended area where the epoxy resin had separated from the surface. Judging from the staining and etching the active reacting surface was at least seven times the size of the two new fracture surfaces.

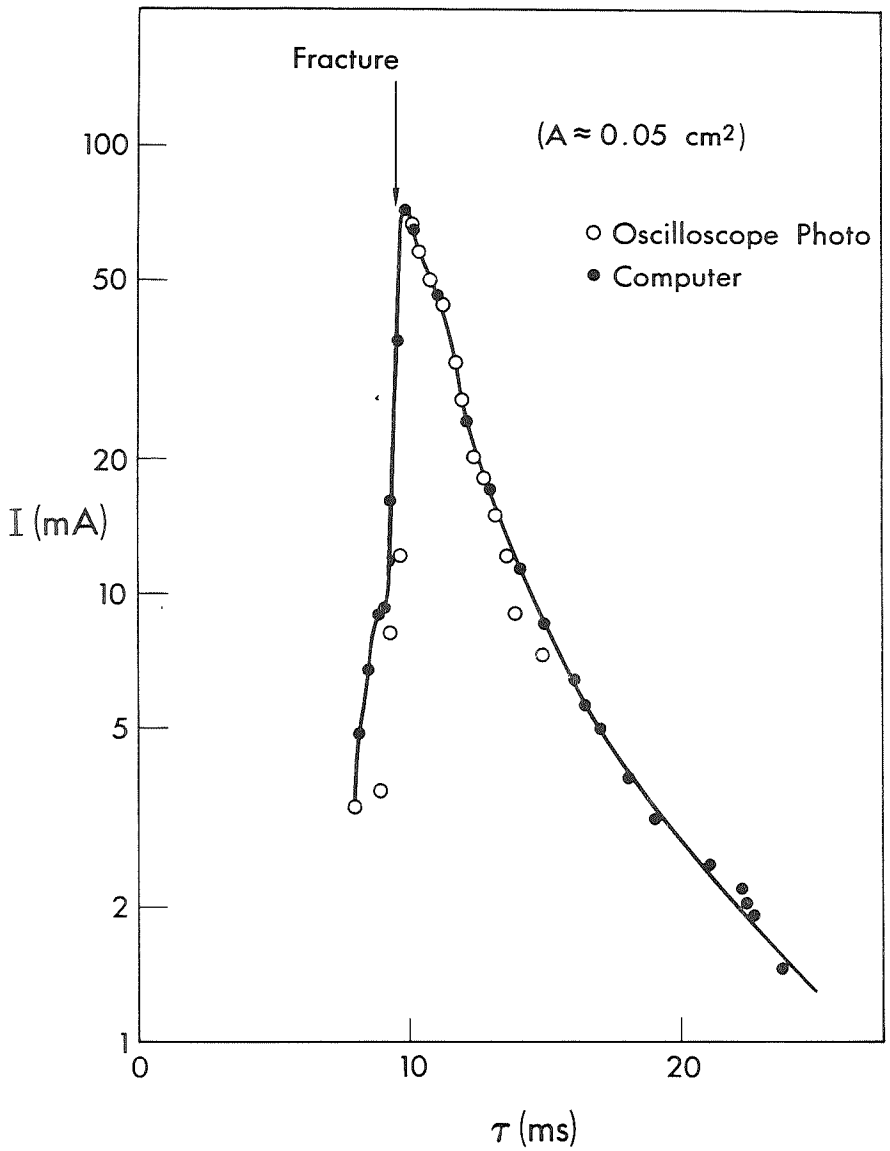

Fig. 1 Kinetic data compiled by computer commercially pure titanium in 3MHCl at -500 mV

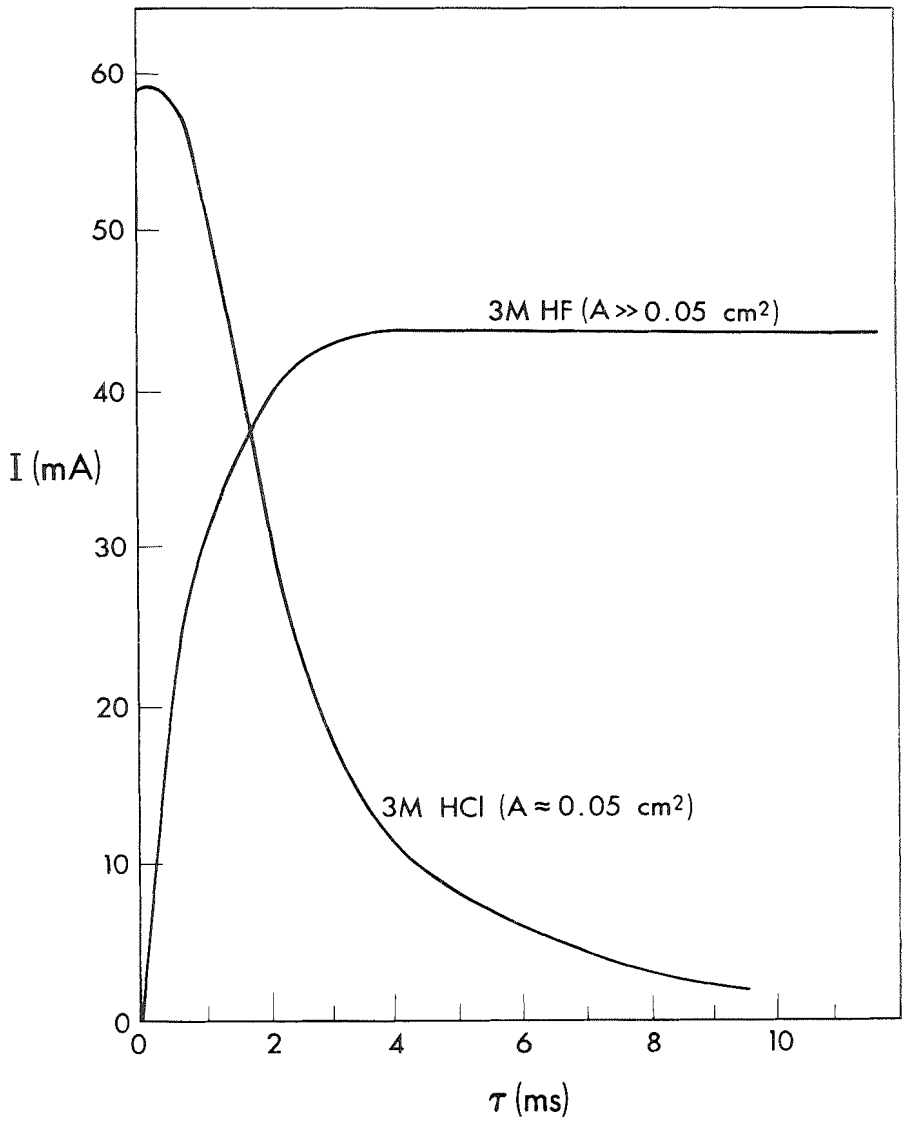

Fig. 2 Current-time curves for new surfaces of commercially pure Ti in HCl and HF at a potential of -500 mV (SCE)

The conductivity of 3 M HF is about 1/35 that of 3 M HCl (18), thus explaining why the plateau current was lower in the HF solution in spite of the larger area. The difference in electrode geometry makes a quantitative comparison of current densities difficult. The current reached the plateau level in less than 4 milliseconds indicating that the air-formed titanium oxide film on the old surface is very rapidly removed by HF.

A current-time curve for a new titanium surface in methanol-HCl solution is shown in Fig. 3. (The solution was prepared by bubbling into anhydrous methanol a stream of HCl gas produced by slowly dripping concentrated H_2SO_4 onto NaCl in a flask. HCl concentration in the methanol was determined by titration of an aliquot with standard NaOH solution.) The new titanium surface did not passivate rapidly as it does in aqueous solutions.

Peak current for new titanium surfaces is plotted in Fig. 4 as a function of potential in varous electrolytes. Whereas the aqueous solutions had mixed potentials at -750 to -800 mv the metahnol - HCl solution had a mixed potential at about -200 mv. This can be attributed to the considerably inhibited cathodic kinetics as noted by the small slope on the cathodic side. In Table 1 it is seen that the apparent resistance of the cell on the anodic side is reasonably consistent between the aqueous and methanol solutions. The apparent resistance is nearly a factor of 10 greater on the cathodic side in metahanol - HCl indicating that the reduction reaction on the surface is inhibited. This strikes a significant blow to the hydrogen model for SCC propagation in methanol because the region II SCC velocity is nearly the same in methanol-halide solutions as in water-halide solutions.

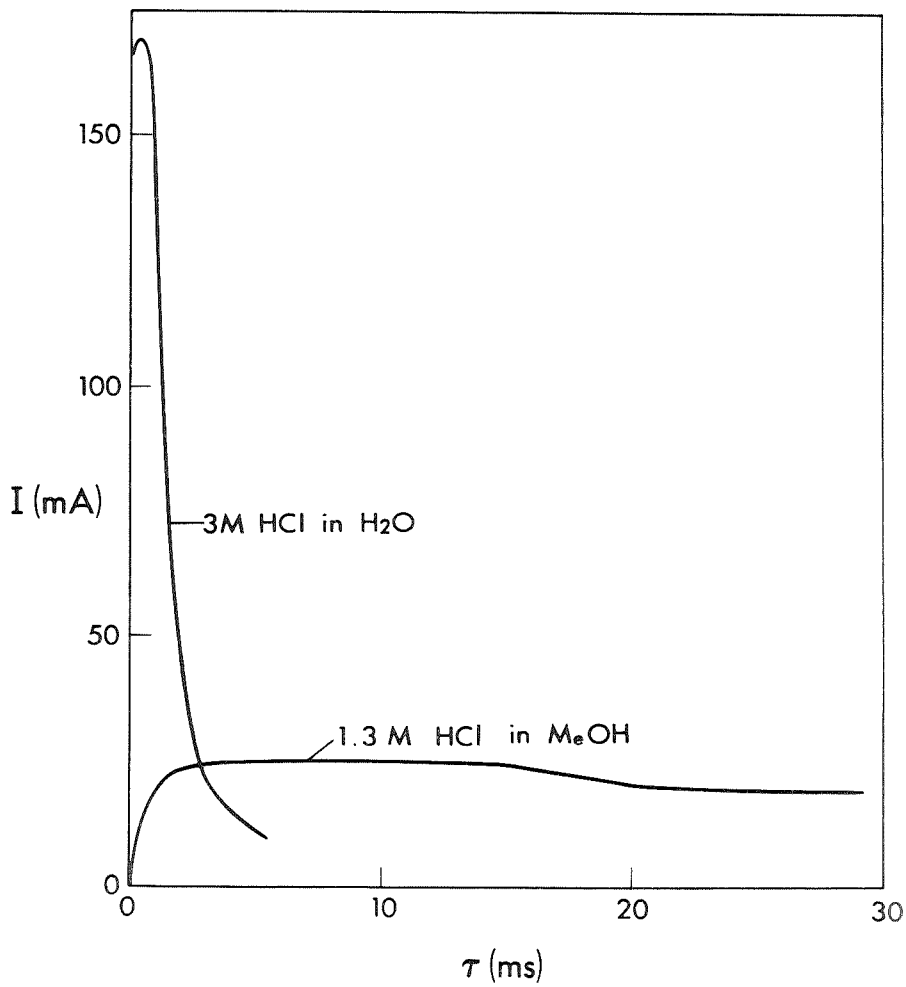

Fig. 3 Current-time curves for new surfaces of commercially-pure Ti in aqueous and methanolic solutions of HCl at a potential of 0 mV (SCE)

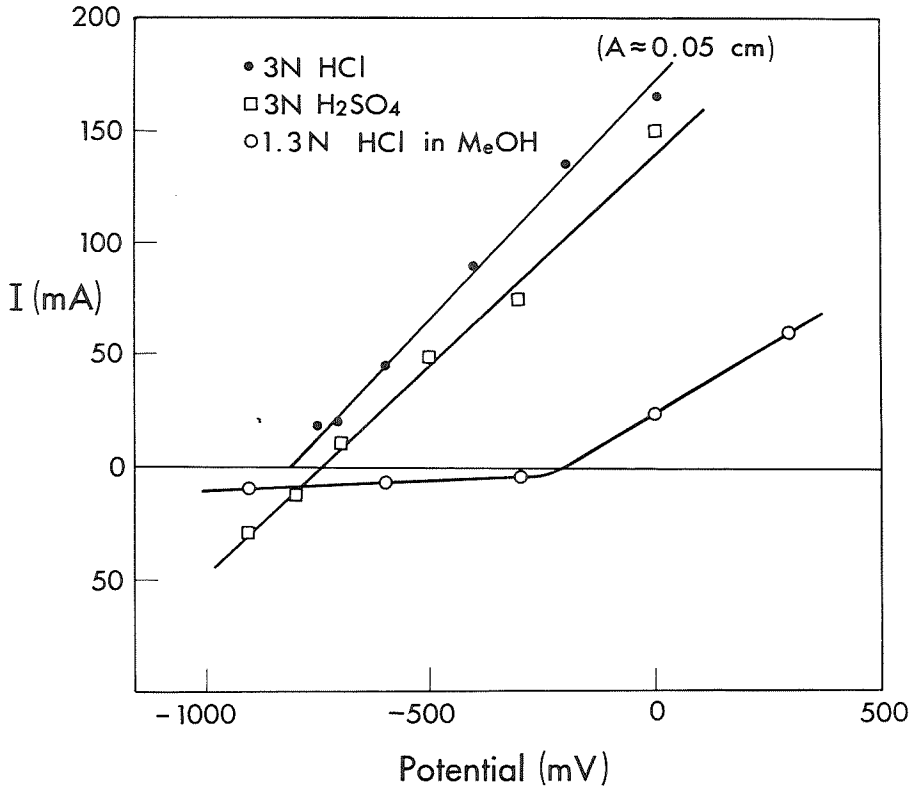

Fig. 4 Peak current for new titanium surfaces as a function of potential in aqueous and methanol solvents

Solution	κ ($ohm^{-1}cm^{-1}$)	R_a(ohm)	R_c(ohm)	R_{calc}*(ohm)	$\frac{R_a}{R_{calc}}$	$\frac{R_c}{R_{calc}}$
3N HCl	0.65	4.6	-	1.9	2.4	-
0.6N KCl	0.066	51	-	19	2.7	-
3N H_2SO_4	0.50	5.3	5.3	2.5	2.1	2.1
1.3 N HCl in MeOH	0.37**	8.3	70	3.4	2.4	20

* $R_{calc} = \frac{1}{2\kappa\sqrt{\pi A}}$ $A = 0.05\ cm^2$ (J. Electrochem. Soc., 115, 890 (1968))

* Valve of κ for aqueous solution - no data for methanol solution

a = anodic

c = cathodic

Table 1 Comparison of Apparent Cell Resistance at Current Peak to Calculated Value

A steady-state polarization curve measured with commercially-pure titanium in the same methanol-HCl solution is shown in Fig. 5. The mixed potential was between -500 and -600 mv in several runs but prolonged cathodic polarization shifted it in the positive direction. It is seen in Fig. 5 that the mixed potential of the new surface is considerably more positive than for the steady-state surface. The corrosion current density is also greater as in aqueous solutions but only by a factor of 10 to 100 as compared to about 10^5 in aqueous HCl solution.

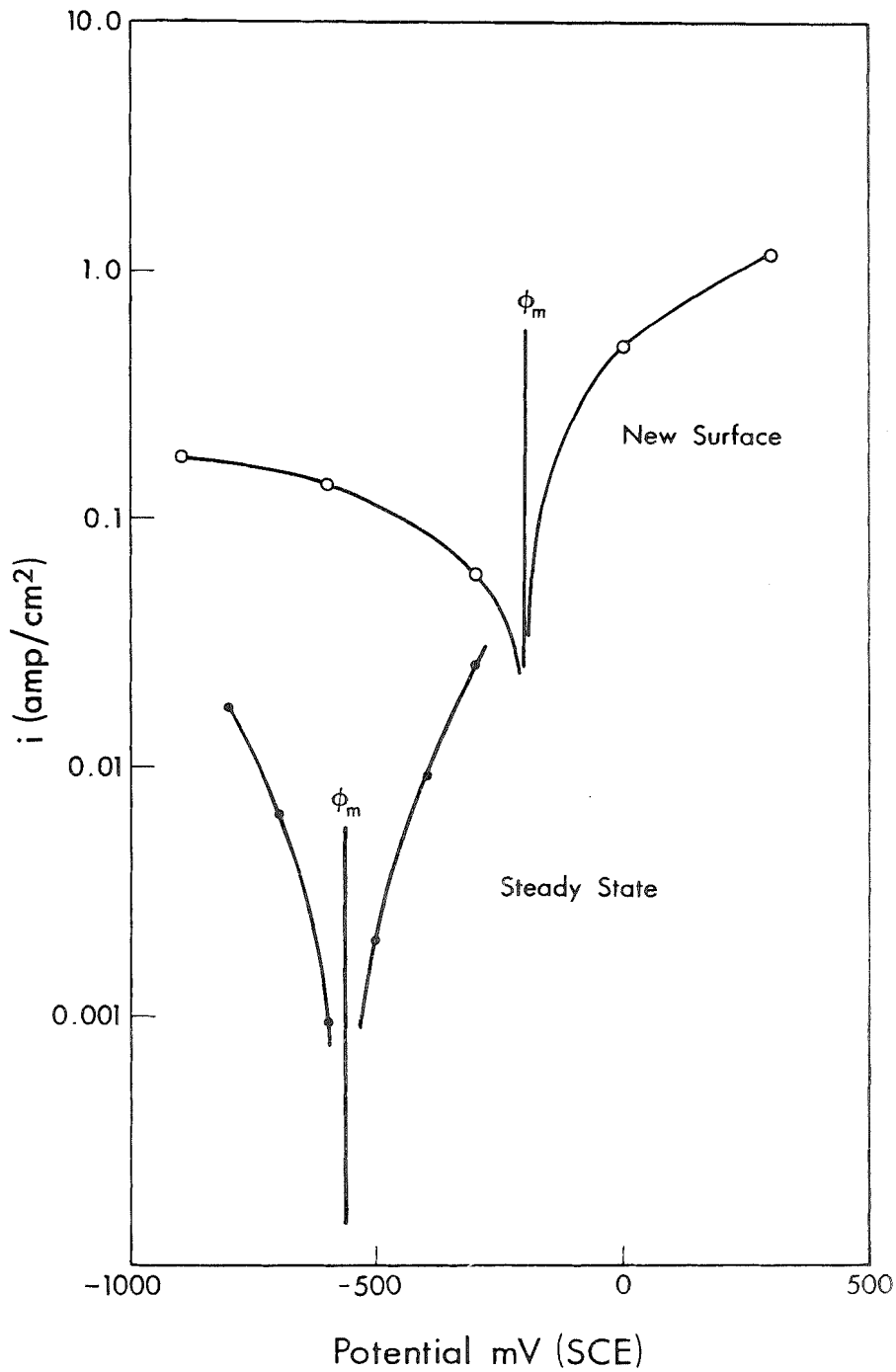

Fig. 5 Polarization curves for new surface and steady-state condition of titanium in methanol-HCl

3.1.2 Analysis of Data

The purpose of conducting the electrochemical kinetics experiments on new surfaces of titanium is to obtain quantitative data that can be used in the electrochemical mass-transport-kinetic (MTK) model for SCC of titanium. The model that appears to fit the kinetic data best at potentials anodic to the mixed potential in HCl solutions is dissolution of titanium to form Ti^{3+} which is inhibited by simultaneous formation of oxide patches (11). The model is illustrated in Fig. 6. The dissolution reaction:

$$Ti \rightarrow Ti^{3+} + 3e$$

is assumed to follow Tafel kinetics

$$i_{+} = i_{o+}(1-\theta) \exp\left[\frac{\alpha nF}{RT} (\phi_s \ \phi_{e+})\right] \qquad 1$$

Assuming instantaneous nucleation and two-dimensional growth, the coverage by oxide patches, θ, can be expressed by

$$\theta = 1 - \exp[-C\tau^2] \qquad 2$$

and the current density to the patches by

$$i_{ox} = 2Q_o C\tau \exp[-C\tau^2] \qquad 3$$

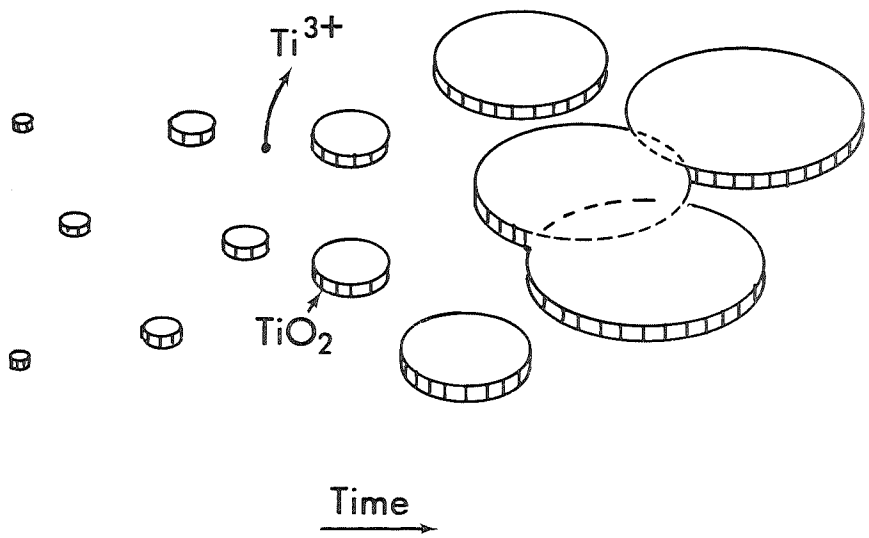

Fig. 6 Illustration of growth of oxide patches with corrosion on bare areas

Substituting equation 2 in equation 1 gives

$$i_+ = i_{o+} \exp[-C\tau^2] \exp\left[\frac{\alpha n}{RT} (\phi_s \ \phi_{e+})\right] \qquad 4$$

A value of the constant, C, was determined that gave an approximate fit of equation 4 to experimental data (11).

A question that arises is, what determines the value of C and is it a constant? From theory (19) it can be shown to be related to the current density at the periphery of the patches by

$$C = \pi n\left(\frac{\delta_m i_2}{Q_o}\right)^2 \qquad 5$$

The value of i_2 might be expected to be some function of applied potential, determined either by Tafel kinetics, mass transport or ohmic drop in solution. A mass transport limit is not probable because the reactant from solution is water which is in high concentration. An analysis given in Appendix I indicates that ohmic drop in the solution in the micro-region around the patches is not limiting. A kinetic limitation at the surface might therefore be expected. The number of patches per square centimeter, n, is assumed to be constant for the present because nucleation occurs at the mixed potential which is assumed to be immediately established when the solution hits the surface after fracture.

As a first approximation to the effect of potential on the value of C, the Tafel part of equation 4 was assumed constant and $C^{\frac{1}{2}}$ was determined from the slope of log current versus τ^2 plots. Results are given in Fig. 7 in which a Tafel plot of $C^{\frac{1}{2}}$ (proportional to i_2 in equation 5) is made. Points are shown calculated for hydrogen ion discharge on the cathodic side of the mixed potential as well as for the anodic side. The value of $C^{\frac{1}{2}}$

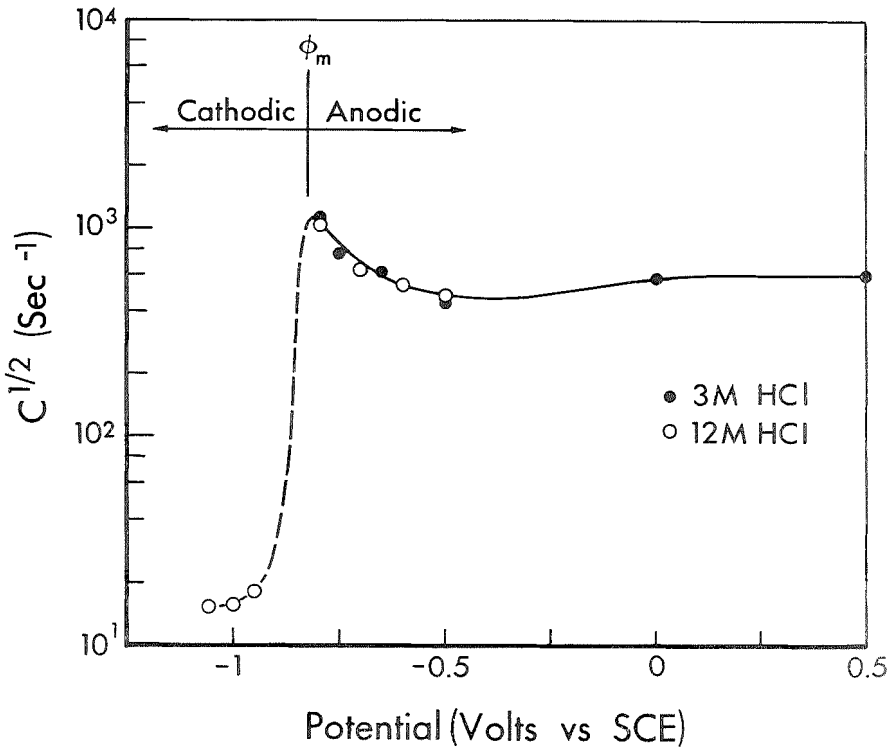

Fig. 7 Tafel plot of $C^{\frac{1}{2}}$ from Equation 4

appears to go through a maximum at about ϕ_m.

The value of the Tafel part of equation 4 cannot be a constant at high overpotentials so a more accurate point-by-point calculation was made. The value of $C^{\frac{1}{2}}$ was solved numerically from the experimental current-time data using the equation

$$C^{\frac{1}{2}} \int_0^{\tau} C^{\frac{1}{2}}\, d\tau = -\frac{1}{2}\left[1 + \left(\frac{\alpha n F \rho \bar{\ell}}{RT}\right) i\right] \frac{d\ell n i}{d\tau} \qquad 6$$

which is derived in Appendix II. The value of $\frac{\alpha n F}{RT}$ was assumed to be 19.5 volts^{-1} (i.e., $n = 0.5$) and $\rho\bar{\ell}$ was calculated from the slope of the experimental peak anodic current density versus potential. The values of $C^{\frac{1}{2}}$ so calculated are plotted versus $(\phi_p - i\rho\bar{\ell})$, the electrode surface potential, in Fig. 8. Comparing to Fig. 7 it is seen that the value of C begins at about the same level at the mixed potential but continues to decrease with increasing potential. It was expected that $C^{\frac{1}{2}}$ might be a unique function of potential of the surface regardless of the potential set on the potentiostat but this expectation was not fulfilled.

If the dissolution current density between patches becomes very large as the surface potential becomes more anodic then it might be expected that "holes" will be corroded between the patches as illustrated schematically in Fig. 9. The oxide monolayer would then have to follow the surface into the holes. Under these circumstances the Avrami condition relating actual coverage to extended coverage does not apply and a new relationship would have to be derived. An equation

$$\frac{d\ell n\left[1-\cos\gamma \int_0^{\tau} C^{\frac{1}{2}}\, d\tau\right]}{d\tau} = \tfrac{1}{2}\left[1 + \left(\frac{\alpha n F \rho \bar{\ell}}{RT}\right) i\right] \frac{d\ell n i}{d\tau} \qquad 7$$

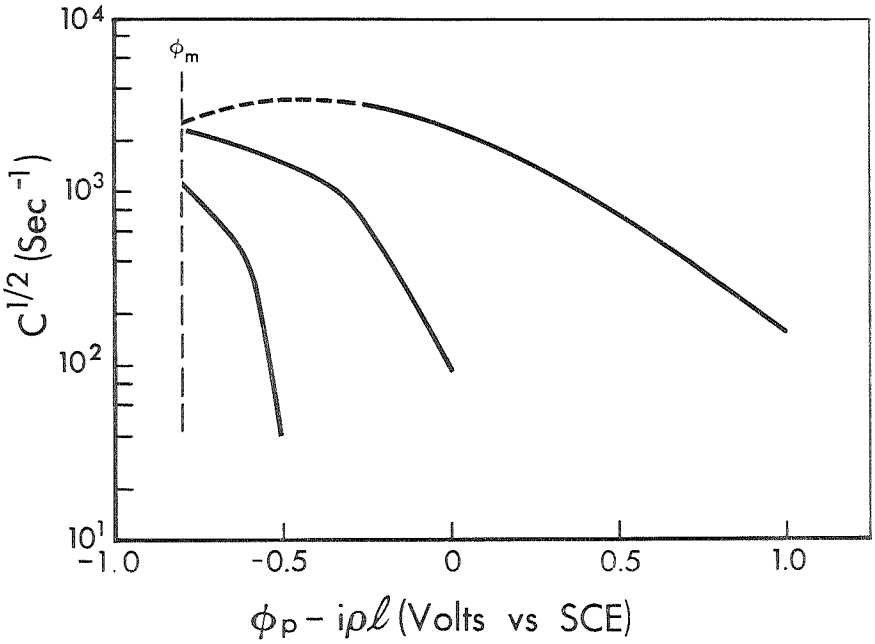

Fig. 8 Value of $C^{\frac{1}{2}}$ as a function of electrode surface potential for three experiments (at ϕ_p = -0.5, 0 and + 1.0 volts) from Equation 6

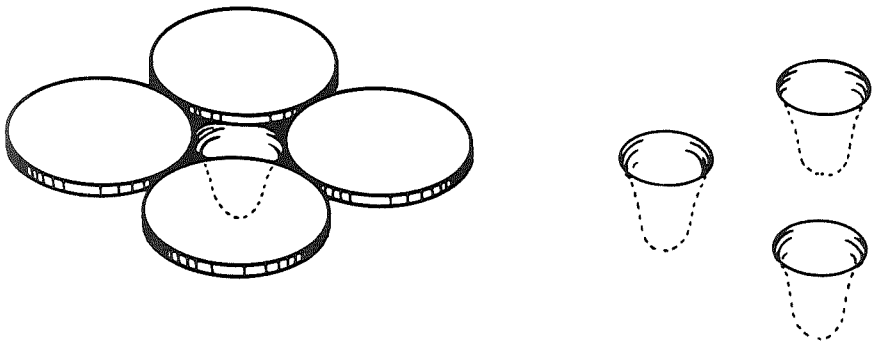

Fig. 9 Schematic representation of holes corroded between oxide patches

was derived for this condition in Appendix III. Values of $C^{\frac{1}{2}}$ were computed from the same data shown in Fig. 8 and plotted in Fig. 10. The value of $\cos\gamma$, (see Appendix III) was assumed to be constant at 1, thus the values of $C^{\frac{1}{2}}$ are minimum values. Data for the three runs fell closer together than for equation 6. The slopes of the lines are about -220 mv per decade of $C^{\frac{1}{2}}$. An interpretation of this negative slope is given in Appendix IV. The concept is that an intermediate is formed at the edge of the patches that can react further to form either the passivating oxide or Ti^{3+} ion. It is considered that the rate of formation of Ti^{3+} increases faster with potential than the rate of formation of passive oxide. A possible reaction scheme is:

$$
\begin{array}{lcl}
 & & + H_2O \xrightarrow{i_2} TiO_2 + 2H^+ + 2e \\
Ti + H_2O & \xrightarrow{i_1} & Ti\,O \quad + 2H^+ + 2e \\
 & & + 2H^+ \xrightarrow{i_3} Ti^{3+} + H_2O + e
\end{array}
$$

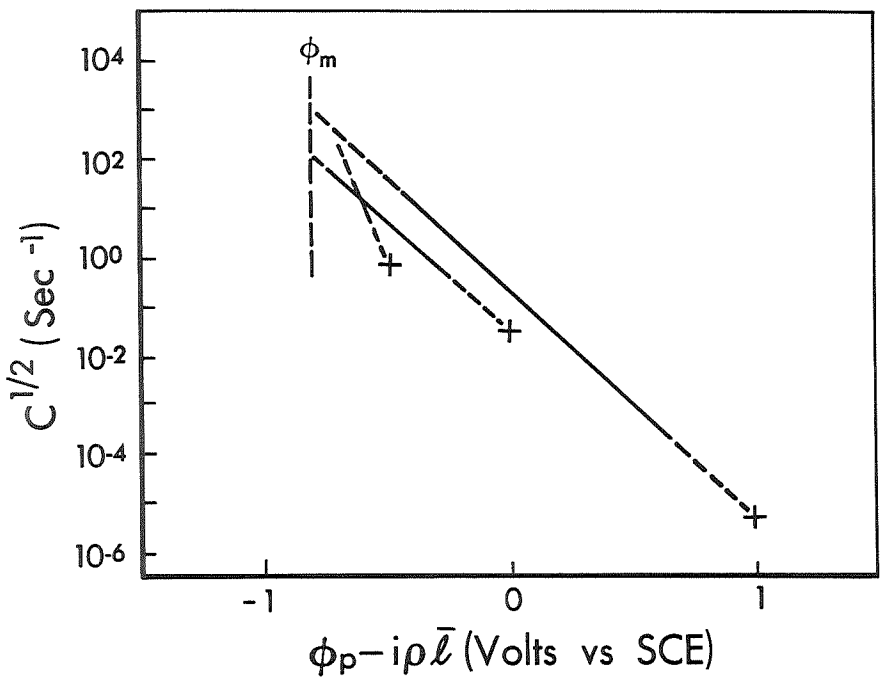

Fig. 10 Value of $C^{\frac{1}{2}}$ as a function of electrode surface potential for three experiments (at ϕ_p = -0.5, 0 and 1.0 volts) from Equation 7

3.2 SCC in Molten Salts

Introduction

Work on stress corrosion cracking in molten salts has been concentrated on the LiCl-KCl eutectic melt since the last progress report (16). It has been directed toward the determination of the effect of H_2O and the influence of temperature on crack propagation behavior, and the elucidation of the role of anodic dissolution on the cracking process. This melt was chosen because:

(1) very dry melts may be obtained;

(2) titanium does not passivate in these melts under anodic dissolution conditions.

The earlier results indicated that hydrogen embrittlement was not important. These results were: (1) visual observations of cracking in melts with and without water revealed no large differences in propagation velocity, and; (2) cathodic protection of the specimen would not be expected if hydrogen embrittlement were important. These qualitative visual results are made quantitative in a later section. The cathodic protection results will be discussed further here in connection with the water concentration in the melts.

Protection of the specimen is achieved by holding it at a potential (with respect to a reference electrode) which is cathodic of the rest potential of titanium. Under these conditions the titanium will not dissolve. This is a strong indication that anodic dissolution plays a major role in the crack extension process. Further, the reduction of hydrogen ions reaches a limit (i.e., a limit caused by diffusion) at a potential which is anodic of the rest potential of titanium, and

one would still have the same amount of hydrogen ion reduction at more cathodic potentials. Therefore, the electrochemical behavior of hydrogen remains constant through the potential range where cracking may be initiated or stopped.

Two major conclusions may be drawn from this. The first is that the very existence of cathodic protection in a region where hydrogen is being evolved indicates that hydrogen is not important in cracking. The second is that hydrogen is not involved since it is being generated at a constant rate in the region where the cracking is discontinuous (i.e., may be initiated or stopped).

The magnitude of the flux of hydrogen ions, at limiting current, is very small in the very dry melts which are available. Thus, it is pertinent to ask what velocity of crack propagation could be supported by the hydrogen in these dry melts. If it is much lower than observed, this would be an additional argument against the necessity for hydrogen to play a major role in the cracking.

The LiCl-KCl eutectic is available commercially as a polaroquality material, with the amount of OH^- specified to be less than 1 ppm*. This would support a limiting current (of hydrogen ion reduction) under ordinary convection conditions given by

$$i_{lim} = \frac{nF z_{H^+} D_{H^+} C_{H^+}}{\delta_{diff}} \cong 10^{-3} \text{ amps/cm}^2$$

---

*Anderson Physics Laboratory

where

n = number of electrons involved in charge transfer = 1

F = Faraday's constant $\approx 10^5$ coulombs

z_{H^+} = charge number of hydrogen ion = 1

D_{H^+} = diffusion coefficient of hydrogen ion = 10^{-5} cm^2/sec

C_{H^+} = concentration of hydrogen ion = 10^{-5} $moles/cm^3$

δ_{diff} = diffusion layer thickness = 10^{-2} cm.

Our measurements of limiting current in these melts are generally about 1/30 of this, i.e., 30 $\mu A/cm^2$. This calculation would be appropriate for a plane interface, and the equivalent calculation for a wedge-shaped crack would be to give an even lower value for the limiting flux to the crack tip. In fact, in the limit of a "sharp" crack tip, the limiting flux would be exactly <u>zero</u> at the crack tip.

To demonstrate this, one may calculate the flux of hydrogen by solving the equation of continuity. In the presence of a large excess of other current carriers (i.e., the - Li^+, K^+ and Cl^- ions) and under steady-state, stagnant conditions (i.e., the solution is pulled along with the crack), the equation of continity becomes

$$\nabla^2 C_{H^+} = 0$$

This equation has the general solution

$$C_{H^+} = a_o + b_o \ln r + (d_o + f_o \ln r)\theta$$

$$+ \sum_k \left(\left[a_k r^k + b_k r^{-k} \right] \cos k\theta \right.$$

$$\left. + \left[d_k r^k + f_k r^{-k} \right] \sin k\theta \right)$$

where C_{H^+} is the concentration of hydrogen ions

r is the distance from the tip of the crack

θ is the angle where one side of the crack is taken as zero

k is the separation constant

a_o, b_o, a_k, b_k, d_o, f_o, d_k, f_k are constants

In order to have symmetry in C_{H^+},

$$d_o = f_o = 0, \; k = \frac{n\pi}{\theta} \quad , \quad n \text{ odd.}$$

In order that

$C_{H^+} = 0$ (i.e., at limiting current) for $\theta = 0$

and $\theta = \theta_1$ (crack angle) for all values of r,

$$a_k = b_k = a_o = b_o = 0.$$

If the crack tip is assumed to be "sharp", one must also have

$$f_n = 0.$$

This gives an equation for C_{H^+} ,

$$C_{H^+} = \sum_{n\,odd} d_n \, r^{n\pi/\theta_1} \sin^{n\pi\theta/\theta_1}$$

where the constants, d_n, are to be determined from other boundary conditions. Without solving the problem any further, it can be seen that

$$\frac{1}{r}\frac{\partial C_{H^+}}{\partial \theta}\bigg|_{\substack{0=0,\\ r\to 0}} = 0$$

(i.e., the flux of hydrogen ions normal to the crack wall)

since $n\pi/_{\theta_1} >> 1$ for the small angle cracks of interest here.

For cracks with rounded tips, the equation for C_{H^+} is,

$$C_{H^+} = \sum_{n\,odd} \left[d_n r^{n\pi/\theta_1} + f_n r^{-\pi/\theta_1} \sin \frac{n\pi\theta}{\theta_1} \right]$$

Here, the crack tip is taken to be at $r = \delta_1$ and the outer opening to the crack is at $r = \delta_2$. For $\delta_1 << \delta_2$, the actual shape of the crack tip would not be expected to be of much importance.

If one uses the boundary conditions

$$C_{H^+} = 0 \quad \text{at } r = \delta_1,$$

$$\frac{\partial C_{H^+}}{\partial r}\bigg|_{r=\delta_2} = -\frac{i_{lim}}{FD_{H^+}}$$

a solution may be obtained. The first boundary condition just states that the hydrogen is being reduced at limiting current at the crack tip. The second boundary condition reflects the amount of current flowing into the crack and is taken to be the same as the limiting current to a plane interface. The solution is

$$C_{H^+} = \left(\frac{4\theta_1}{\pi^2}\right)\left(\frac{i_{lim}}{FD_{H^+}}\right)\sum_{n\,odd}\frac{1}{n^2}\left[\frac{r^{n\pi/\theta_1} + (\delta_1^{2n\pi/\theta_1})\, r^{-n\pi/\theta_1}}{\delta_2^{n\pi/\theta_1-1} - (\delta_2^{-n\pi/\theta_1-1})\,\delta_1^{2n\pi/\theta_1}}\right]\sin\frac{n\pi\theta}{\theta_1}$$

The current to the tip (i.e., $r = \delta_1$) is,

$$\left.\frac{\partial C_{H^+}}{\partial r}\right|_{r=\delta_1} = -\left(\frac{8}{\pi}\right)\left(\frac{i_{lim}}{FD_{H^+}}\right)\sum_{n\,odd} + \frac{\sin\frac{n\pi\theta}{1}}{n}\left(\frac{\delta_1^{n\pi/\theta_1}}{\delta_2^{n\pi/\theta_1-1} - (\delta_2^{n\pi/\theta_1-1})\,\delta_1^{2n\pi/\theta_1}}\right)$$

In the situation where

$$\delta_1 << \delta_2$$

$$\left.\frac{\partial C_{H^+}}{\partial r}\right|_{r=\delta_1} \cong \left(\frac{8}{\pi}\right)\left(\frac{i_{lim}}{FD_{H^+}}\right)\sum_{n\,odd}\frac{\sin\frac{n\pi\theta}{\theta_1}}{n}\left(\frac{\delta_1}{\delta_2}\right)^{-\frac{n\pi\theta}{\theta_1}-1} .$$

The largest term of the series is the first. If

$$\frac{\delta_1}{\delta_2} \approx 10^{-3}\ ,\ \frac{\pi}{\theta_1} = 90\ ,\quad \theta = \frac{\theta_1}{2}\ ,$$

$$\left.\frac{\partial C_{H^+}}{\partial r}\right|_{\substack{r=\delta_1,\\ \theta=\frac{\theta_1}{2}}} \cong -\left(\frac{8}{\pi}\right)\left(\frac{i_{lin}}{D_{H^+}}\right)\left(10^{-3}\right)^{89}$$

and the tip current due to hydrogen ion reduction is extremely small as compared to the current to bulk surface. Virtually the same conclusion is reached if the second boundary condition is taken as

$$\left.\frac{\partial C_{H^+}}{\partial r}\right|_{r=\delta_2} = -\frac{i_{lim}}{FD_{H^+}} \quad \text{at } \theta = \frac{\theta_1}{2} \qquad \text{i.e.,}$$

$$\left.\frac{\partial C_{H^+}}{\partial r}\right|_{r=\delta_1} = \frac{2\left(\frac{i_{lim}}{FD_{H^+}}\right)\delta^{\pi/\theta_1-1}\sin\frac{\pi\theta}{\theta_1}}{\delta_2^{\pi/\theta_1-1}(\delta_2-\pi/\theta_1)\delta_1^{2\pi/\theta_1}}$$

For the case, again,

$$\delta_1 << \delta_2, \frac{\delta_1}{\delta_2} = 10^{-3}, \quad \frac{\pi}{\theta_1} = 90, \theta = \frac{\theta_1}{2},$$

$$\left.\frac{\partial C_{H^+}}{\partial r}\right|_{r=\delta_1} = -2\left(\frac{i_{lim}}{FD_{H^+}}\right)\left(\frac{\delta_1}{\delta_2}\right)^{\pi/\theta_1-1}$$

$$= -2\left(\frac{i_{lim}}{FD_{H^+}}\right)\left(10^{-3}\right)^{89}$$

This conclusion, that there is a negligible tip current due to hydrogen ion reduction means that the velocity of crack propagation which may be supported by hydrogen embrittlement is negligible. The result could be moderated by introducing convection, but this would not be expected to produce a major change in the conclusion.

The final point to be made in this report concerning the influence of hydrogen embrittlement on stress corrosion cracking in molten salts is the comparison of behavior in "wet" and "dry" melts. In order to determine the effect of water concentration on the crack behavior, one must first consider the range of water solubility available for study, and methods of determining the concentration of water in the melts. Burkhard and Corbett (20) have determined the solubility of water in LiCl-KCl melts as a function of temperature and water vapor pressure. As in other melts (21), the solubility was found to be a linear function of vapor pressure at low pressures. At partial pressures of H_2O above ~ 15 mm (depending on temperature), the solubility was found to depart from the Henry's Law behavior, with the generation of HCl by hydrolysis. The Henry's Law constant at 390°C was determined to be 30.0 and 30.5 mole H_2O (mole LiCl)$^{-1}$ mm^{-1} at 50 mole % and 60 mole % LiCl, respectively (the eutectic is 58 mole % LiCl). This corresponds to 9.7 and 9.8 ppm (mm)$^{-1}$ respectively. If the melt were to achieve equilibrium with the dry box atmosphere (10^{-5} mm H_2O), the melt would contain the minimum amount of water we can attain, i.e., 9.7×10^{-5} ppm H_2O at 390°C. The maximum water content obtainable without appreciable hydrolysis would be 136 ppm at this same temperature. This maximum water content is approximately two orders of magnitude higher than in the commercial melts.

There are additional and more serious limitations caused by the glassware used in the experiments. That is, when water is introduced into a LiCl-KCl melt, the glassware reacts with the melt. This "etching"

does not cause any problems in obtaining data, as long as the wall is wet by the melt. But the reaction with glass does render the concentrations of various species in the melt to be variable with time - which is of course undesirable. The uncertainty associated with the introduction of impurities from the etching is also undesirable.

The various reactions which may occur and the relative importance of each is outlined below. The thermodynamic properties of the species were taken from the literature (22). Although the experiments were not conducted at standard conditions, which are the conditions used in the calculations, the major conclusions are not affected. At 700°K,

(1) $LiCl(\ell) + H_2O(g) \rightleftarrows LiOH(\ell) + HCl\ (g) \quad \Delta G° = +19$ kcal

(2) $KCl\ (\ell) + H_2O(g) \rightleftarrows KOH(\ell) + HCl\ (g) \quad \Delta G° = +36$ kcal

(3) $H_2O\ (g) + 2\ LiCl(e) + SiO_2(s) \rightleftarrows Li_2SiO_3(\ell) + 2\ HCl(g)$

$\Delta G° = +\ 8$ kcal

(4) $2H_2O(g) + 2LiCl(\ell) \rightleftarrows Li_2O_2(\ell) + 2HCl\ (g) + H_2(g)$

$\Delta G° = +45$ kcal

(5) $2H_2O(g) + LiCl(\ell) \rightleftarrows Li_2O(\ell) + 2HCl\ (g) \quad \Delta G° = +60$ kcal

Reactions (1), (2), (4), and (5) are reactions between water and the melt components. Reaction (3) includes the glass as a reactant. Therefore, in melts equilibrated with water, in glass, it would be expected that the metasilicate (Li_2SiO_3), LiOH, and HCl would be major hydrolysis products. KOH, Li_2O_2, and Li_2O would be very minor species. Further, Li_2SiO_3 would

probably be in higher concentration in the melt than LiOH. Other reactions may involve the pyrex components Na_2O and B_2O_3, with consequent introduction of other contaminants into the melt.

These calculations serve to indicate that it will not be possible to go to as high water concentrations in glass containers as in an inert container (such as Pt). Alternatively, in order to conduct experiments on the effect of high concentrations of H_2O on SCC, it would be necessary to use an inert container such as boron nitride. This would introduce problems of obtaining data, since the specimen could not be observed as easily as in glassware.

The measurement of water concentration in LiCl-KCl melts has been done by two methods in the past. Burkhard and Corbett (20) used an absolute pressure method to determine the amount of water taken up by their melts. Laitenen and others (23) have used an electrochemical method, i.e., residual current measurements, to determine the relative amount of water in their melts. There is no report in the literature of an attempt to measure the absolute quantity of water in these melts by the electrochemical method, but such an investigation would be very useful*. In the present investigation, residual currents have been measured to determine relative concentrations of water.

---

*Anderson Physics Laboratory uses residual current measurements to indicate water contents in their product but there are no details in the literature.

Results

Results have been obtained for stress corrosion cracking in both "wet" and "dry" melts. In Fig. 11 are the data for 375°C. The data for melt (I) were given in the previous progress report (16) and are given again here for purposes of comparison. In that report, it was noted that the data were taken at -900 mV. A different reference electrode was used for the data obtained with melt II. By comparison of the reference electrodes, it was possible to put the data from melt I on the same potential scale. The data for melt (II) were obtained in an eutectic which was Polaroquality* and was specified to contain less than 1 ppm hydrogen (as OH^-). By comparison of the "residual" current from the polarization curves for each melt, melt (I) was found to contain approximately 10 times more hydrogen than melt (II). It is seen that in the plateau region, and in the stress-dependent region (at low stresses) the two sets of data coincide. We are unable to report data for dry melts in the transition region because of the loss of information from several runs (bad movies).

The polarization curve for Ti dissolution in a pure melt has been included in the figure. It serves to indicate that the potential at which all these data were taken was anodic of the rest potential of Ti. In both melts (I) and (II), the specimen could be cathodically protected. The crack may be initiated by switching to an anodic potential, and stopped by switching back to a cathodic potential. The velocity of crack propagation in the stress independent region is independent of the anodic potential, so far as it has been possible to determine. In the stress dependent region, at a constant stress intensity, the crack propagates faster the more anodic the potential. The quantitative determination of this potential dependence, in both regions of cracking, is of major interest and will be investigated in the immediate future.

*Anderson Physics Laboratory

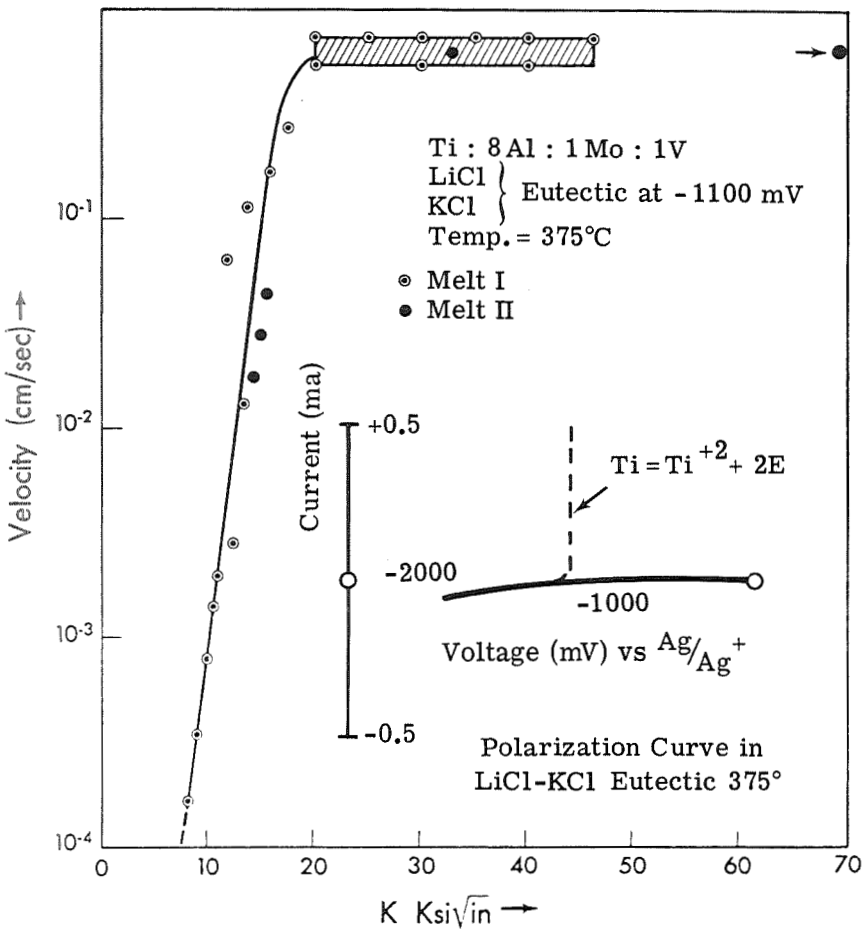

Fig. 11 Velocity as function of stress intensity

Experiments have been conducted in melts with water concentrations approximately 50 times higher than the Polaroquality melt - as determined from residual current measurements. In these melts, contrary to results in the previous melts (I) and (II), it was not possible to cathodically protect the specimen. This precluded taking other data in the melt. These experiments were conducted in glass apparatus and will be repeated in an inert apparatus. The water concentration was such that the glass would have reacted with the melt to introduce contamination. The results obtained for the effect of H_2O concentration on SCC are:

(1) Melts (I) and (II) which differed in water content by an order of magnitude had identical log V vs K curves in the plateau, and at low stress intensities;

(2) In both melts (I) and (II), it was possible to cathodically protect the specimen, and;

(3) In melt (III), with a water content approximately 50 times higher than melt (II), we were unable to cathodically protect the specimen.

Results of experiments designed to reveal the temperature dependence of stress corrosion cracking are given in Figure 12. In this figure is given the velocity of crack propagation <u>in the plateau region</u> as a function of temperature. It has not been possible to determine the analogous temperature effect in the stress-dependent region because of the scatter of data. The trend observed is just outside our experimental uncertainty, and the "activation energy" is found to be about 3 kcal. This is of the same order of magnitude as found for other environments (e.g. 16), and has the same temperature dependence as transport phenomena.

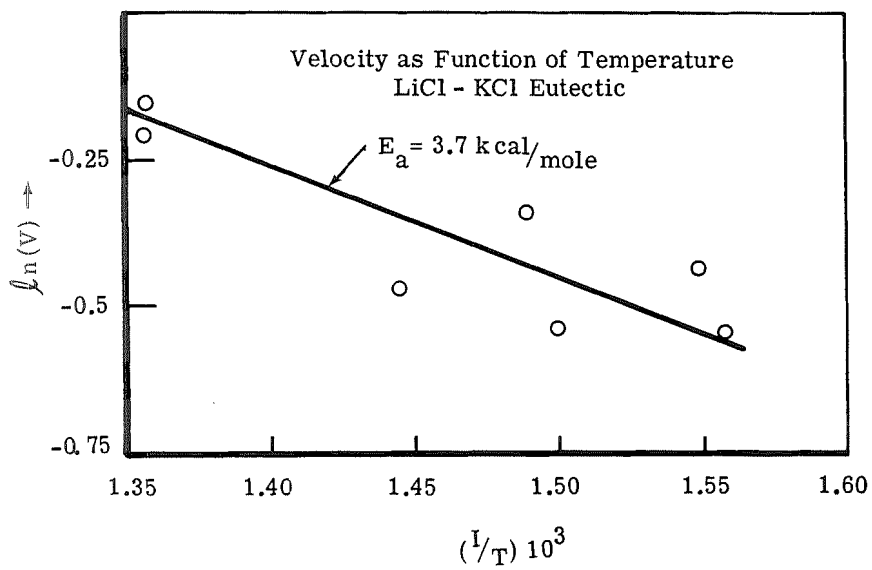

Fig. 12 Velocity as function of temperature for Ti(8%Al, 1%V, 1%Mo) in LiCl-KCl eutectic

Since the results reported so far indicate that anodic dissolution plays a major role in crack propagation in these melts, it is appropriate to describe other results which relate to the anodic dissolution process. These are qualitative at present, but have the prospect of yielding more quantitative data.

There is anodic dissolution from the bulk surface of a specimen during crack propagation. But the pertinent question is whether there is dissolution in the crack itself, and how it is distributed. The first result which indicates that there is indeed anodic dissolution in the crack is the visual observation that the solution in the crack is highly colored (dark green from Ti^{+2}) while the outer solution remains colorless. Of course, the outer solution becomes colored after extensive dissolution, but this takes much longer and one may run several tests in the same melt before the green color may be detected. Also, experiments have been conducted in which the potential of a specimen is changed slowly from the cathodic protection region to more anodic potentials. In a very dry melt, there is no cracking until the current becomes anodic. When cracking starts, there is a simultaneous jump in the current (more anodic) which then decays back to a low level. Data from a current-time trace is given in Fig. 13. It may be seen that the increase is very sharp and cannot be resolved on this trace. The decay of current can be divided roughly into two regions:

(1) initially the current decreases approximately proportional to the inverse of time, and;

(2) then the current decays inversely with the square root of time.

Attempts to directly correlate this current trace to the crack extension rate have been unsuccessful.

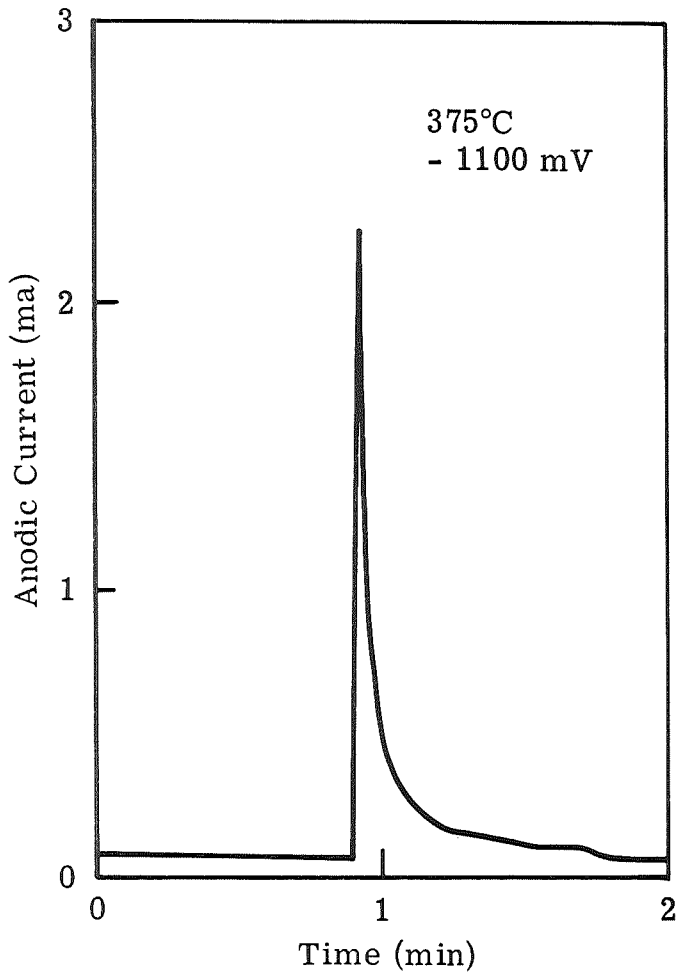

Fig. 13 Current as a function of time at initiation of cracking (Ti(8%Al, 1%V, 1%Mo) in LiCl-KCl eutectic)

Conclusions & Summary

All of the results thus far are consistent with the proposal that hydrogen embrittlement is not responsible for SCC in molten LiCl-KCl eutectics. Further, anodic dissolution does seem to be involved in the fracture. We base these conclusions on the observations in melts with low water content, i.e.,

(1) the water (or hydrogen) content is too low to support cracking of the velocities observed;

(2) it is possible to prevent cracking, and to stop it once started, by maintaining the specimen cathodic of the rest potential;

(3) crack velocities are a function of potential in the stress dependent region, with the velocity being higher at more anodic potentials;

(4) melts I and II have identical curves of log V vs K over most of the curve;

(5) the more concentrated solution of Ti^{+2} in the crack, indicates a higher rate of dissolution there than on the outer surface;

(6) the current transients at the onset of cracking reveal that anodic dissolution, at a higher level than from the bulk surface, occurs in the crack.

The behavior in melts with higher water content, i.e., no cathodic protection, must be confirmed before speculating about it.

If anodic dissolution alone were responsible for crack propagation at velocities of 7×10^{-1} cm/sec, a tip dissolution current density of about 10^4 amps/cm^2 would be required. By comparing this to the current density on

the outer surface (about 1 ma/cm^2) one sees that the current density would have to be increased by seven orders of magnitude in the crack over that on the outer surface. Part of this effect could be caused by the "clean" nature of the crack walls, since Ti does not passivate in the melt.

It is known from results in this laboratory that the electrochemical behavior of "clean" surfaces is strikingly different from that of partially oxidized surfaces. Indeed, in aqueous solutions Ti exhibits about four orders of magnitude difference in dissolution current at the mixed potential between the two kinds of surface. This is probably the major reason for the higher dissolution current in the crack, as indicated by both the visual observations and the current-time trace. Differences between clean and passivated surfaces cannot totally explain the observed behavior, if anodic dissolution is supposed to occur at the crack tip, however.

If one assumes that the crack walls are not passivated, then one may calculate the expected current distribution. Wagner (24) and Cheh (25) have both solved for the current distribution for case of an electrode with a wedge shaped notch in it. They find that for the primary current distribution, one would expect zero tip current in a sharp crack*. This distribution only takes account of ohmic effects. When the interfacial effects are taken into account through the electrode kinetics, the secondary current distribution is obtained. They find that for linear polarization,

---

*The equation to be solved for the primary current distribution is $\nabla^2\phi = 0$, with appropriate boundary conditions. This equation for the potential is analogous to the equation for C_{H^+} discussed in an earlier section.

$$\frac{i_o - i_t}{i_{avg}} = \frac{L}{K} \frac{di}{d\eta_s} \left(\frac{1}{2}\right) \frac{\cos\left(\frac{\theta}{2}\right)}{\sin^2\left(\frac{\theta}{2}\right)}$$

and for Tafel polarization,

$$\left(\frac{i_o}{i_t}\right) = \frac{|i_{avg}| L(1-\alpha) nF}{KRT} \left(\frac{1}{2}\right) \frac{\cos\left(\frac{\theta}{2}\right)}{\sin^2\left(\frac{\theta}{2}\right)}$$

where i_o is the current density to the crack wall at the entrance

i_t is the current density to the tip of a sharp crack

i_{avg} is the average current density in the crack for the primary current.

$|i_{avg}|$ is the absolute value of the current density in the crack

L is the crack opening, or displacement, at the entrance.

K is the solution conductivity

$(1-\alpha)$ is a kinetic parameter

η_s is the surface overpotential

θ is the crack angle

n is the number of electrons involved in the electrochemical reaction

F is Faraday's constant

R is the gas constant

T is the absolute temperature.

Both of these expressions indicate that the dissolution current density at the tip would not be zero, but would be less than the current density to the outer part of the crack. This is just the opposite of what is needed to extend a crack. Therefore the effect of having clean crack walls would be to distribute the current away from the tip, producing a blunted crack. The only way the tip current could be higher than the current to the outer walls is through an effect of the stress at the tip. This stress might be imagined to change the dissolution kinetics at the tip as well as the potential of zero current. It has been proposed (26) that the application of stress does indeed increase the rate at which dissolution of a metal may occur, but no data has ever been reported on clean, i.e., oxide-free surfaces. There would be great interest in obtaining such data.

The dissolution of titanium seems to be of importance in understanding the observed stress corrosion behavior. From literature data (27), one may calculate the amount of both Ti^{+2} and Ti^{+3} in solution in equilibrium with the metal, i.e.,

$$2Ti^{+3}(soln) + Ti(s) = 3Ti^{+2}(soln).$$

The equilibrium constant for the reaction has the value of

$$K = \frac{[Ti^{+2}]^3}{[Ti^{+3}]^2} \approx 10^6$$

which reveals that Ti^{+3} will always have a lower equilibrium concentration than Ti^{+2}. Therefore, we propose that the dissolution of Ti is primarily due to the reaction

$$Ti(\alpha) \rightarrow Ti^{+2}\ (soln) + 2e^{-}$$

The green solutions formed in our experiments confirm that this reaction does occur but there are no kinetic data for this particular reaction in the LiCl-KCl eutectic. Other divalent ions are formed with exchange current densities of about $10A/cm^2$(28). The reaction

$$Ti^{+2}_{(soln)} \rightarrow Ti^{+3}_{(soln)} + e^{-}$$

has an exchange current density of $40A/cm^2$ (28).

If a limitation of this dissolution is responsible for the stress-independent plateau in the log V vs K curves, it is proposed that this may be a current limited by solid solubility (or some other equilibrium constraint).

In summary, data have been obtained for stress corrosion cracking of Ti(8% Al, 1%V, 1%Mo) in the eutectic melt. These results are consistent with the proposal that hydrogen embrittlement does not play a major role in the cracking process. Further, anodic dissolution seems to be involved in the cracking, and some conclusions have been drawn from this assumption.

4.0 CONCLUSIONS

1. New surfaces of titanium formed in aqueous HF and methanol-HCl solutions showed no evidence of passivation.
2. Model relations for rate of oxide patch growth on new titanium surfaces as a function of potential were derived.
3. Analysis of hydrogen ion transport in molten salt in a stress corrosion crack indicated that the process is too slow for hydrogen to contribute significantly to crack propagation.
4. Experimental evidence of higher dissolution rate of titanium in the propagating crack as compared to the outer surfaces was observed.

5.0 FUTURE WORK

The following items of work are planned for the immediate future:

1. Conduct further SCC studies in molten salts.
2. Conduct further studies on initiation and propagation processes in very large grained specimens of Ti:10Al, Ti:8Mn, Ti:13V11Cr3Al.
3. Study susceptibility to SCC of Ti:Cu, Ti:Al-Si, Ti:V, Ti:16 Mn, and Ti:Sn alloys in various solutions.
4. Resolve the problem of chloride analysis of titanium.
5. Conduct more quantitative electrochemical kinetic studies with a wider range of halide concentrations and potentials for titanium and aluminum.
6. Include parallel soluble titanium ion formation in mass-transport-kinetic model.
7. Focus attention conceptually and experimentally on events at the crack tip.

6.0 REFERENCES

1. T. R. Beck, Boeing Document D1-82-0554, July 1966.
2. T. R. Beck and M. J. Blackburn, Research Proposal D1-82-0467, August 1965.
3. T. R. Beck, Contract NAS7-489, Quarterly Progress Report No. 1, September 1966.
4. Ibid, No. 2, January 1967.
5. Ibid, No. 3, April 1967.
6. Ibid, No. 4, July 1967.
7. Ibid, No. 5, October 1967.
8. Ibid, No. 6, January 1968.
9. Ibid, No. 7, April 1968.
10. Ibid, No. 8, July 1968.
11. Ibid, No. 9, October 1968.
12. Ibid, No. 10, January 1969 (short letter report).
13. Ibid, No. 11, April 1969.
14. Ibid, No. 12, July 1969 (short letter report).
15. Ibid, No. 13, October 1969 (short letter report).
16. Ibid, No. 14, January 1970.
17. Ibid, No. 15, April 1970 (short letter report).
18. International Critical Tables, VI, McGraw Hill, New York, 1933.
19. M. Fleischmann and H. R. Thirsk, in Advances in Electrochemistry and Electrochemical Engineering, Vol. 3, p. 123, P. Delahay and C. W. Tobias, Eds., John Wiley, New York, 1963.

20. W. J. Burkhard and J. D. Corbett, "The Solubility of Water in Molten Mixtures of LiCl and KCl," J. Amer. Chem. Soc. 79, 6361 (1957).

21. F. R. Duke and A. S. Doan, Jr., "The Solubility of Water Vapor in Fused Alkali Nitrate Mixtures and in Lithium Perchlorate," Iowa State College Journal of Science 32, 451 (1958); T. B. Tripp and J. Braunstein, "Vapor Pressures of Aqueous Melts. Lithium Nitrate-Potassium Nitrate-Water at 119-150°," J. Phys. Chem. 73, 1984 (1969); H. S. Hull and A. G. Turnbull, "Thermodynamics of Molten Salt-Water Mixtures. I. Solubility of Water Vapor in a Potassium Nitrate-Sodium Nitrite Melt," J. Phys. Chem 74, 1783 (1970).

22. JANAF Thermochemical Data.

23. H. A. Laitinen and W. S. Ferguson and R. A. Osteryoung, "Preparation of Pure Fused Lithium Chloride-Potassium Chloride Eutectic Solvent," J. Electrochem. Soc. 104, 516 (1957); S. Okada, M. Kawane, and T. Hashino, "Zur Kenntnis der Electrolyse von Titanchlorid in geschmolzenen Salzmischungen," Z. Electrochem. 62, 437 (1958).

24. C. Wagner, "Theoretical Analysis of the Current Density Distribution in Electrolytic Cells," J. Electrochem. Soc. 98, 116 (1951).

25. H. Y. Cheh, "Current Distribution During the Electrodeposition of Gold," J. Electrochem. Soc. 117, 609 (1970).

26. A. R. Despic, R. G. Raicheff and J. O'M. Bockris, "Mechanism of the Acceleration of the Electrodic Dissolution of Metals during Yielding under Stress," J. Chem. Phys. 49, 926 (1968).

27. J. A. Plambeck, "Electromotive Force Series in Molten Salts," J. Chem. Engr. Data 12, 77(1967).

28. G. J. Janz, Molten Salts Handbook, Academic Press (N.Y.) 1967.

29. K. J. Vetter, Berichte der Bunsengesellschaft für Physikalische Chemie, 69, 683 (1965)

7.0 APPENDIX

Appendix I

What determines i_2 at edge of patches.

1. IR drop - calculated here
2. Tafel kinetics - See Appendix IV
3. Mass transport - not likely for $Ti + 2H_2O \rightarrow TiO_2 + 4H + 4e$ because H_2O is at high concentration.

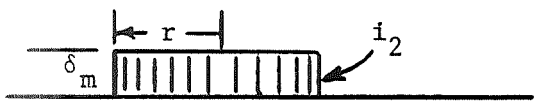

Calculation of IR drop

(initial) (middle) (final)

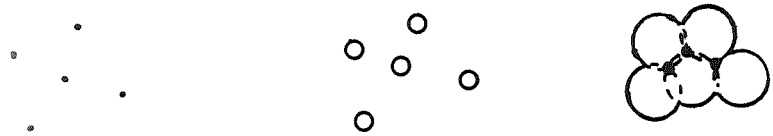

Starts at points with hemispherical conduction

Ends at points with hemispherical conduction

1. Initial Condition

$$\Delta\phi_o = \frac{I_2\rho}{2\pi}\left(\frac{1}{r_1} - \frac{1}{r_2}\right)$$ for hemispherical conduction

$$I_2 = i_2(2\pi\ r_1\delta_m)$$

assume $r_2 >> r_1$

$$\therefore\ \Delta\phi_o = \frac{i_2(2\pi r_1\delta_m)\rho}{2\pi}\left(\frac{1}{r_1}\right) = \rho\delta_m i_2$$

For $\rho = 2$ ohm cm for concentrated HCl,

$\delta_m = 5 \times 10^{-8}$ cm, and

$i_2 = 100$ amp/cm^2;

$\Delta\phi_o = (2)(5 \times 10^{-8})(100) = 10^{-5}$ volts.

$\therefore$ ohmic drop not limiting initially.

2. Middle Condition

There should be smaller IR drop because cylindrical conduction to periphery varies as $\ln(r_2/r_1)$.

3. Final Condition

$$\Delta\phi_o = \frac{(I_2 + I_+)\rho}{2\pi}\left(\frac{1}{r_1} + \frac{1}{r_2}\right)$$

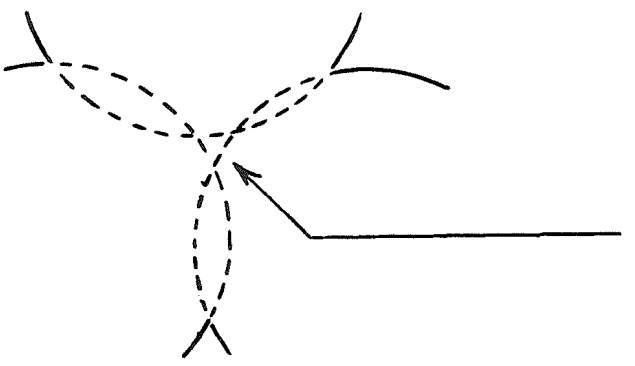

Assume hole has some effective radius, r_1, and $r_2 >> r_1$.

$$I_2 = i_2(2\pi r_1 \delta_m)$$

$$I_+ = i_+(\pi r_1^2)$$

$$\therefore \Delta\phi_o = \frac{i_2(2\,\delta_m) + i_+(r_1)\rho}{2}\rho = (i_2\delta_m + i_+\frac{r_1}{2})\rho$$

Assuming that $r_1 > \delta_m$ and $i_2 \approx i_+$,

$$\Delta\phi_o \approx i_+ r_1 \rho/2.$$

For $i_+ = 1$ amp/cm^2 (for $\tau = 2$ ms @ 0mv in 3M HCl),

$\rho = 2$ ohm cm, and

$r_1 = 2 \times 10^{-6}$cm;

$$\Delta\phi_o = \frac{(1)(2 \times 10^{-6})(2)}{2} = 2 \times 10^{-6} \text{ volts.}$$

∴ Under no condition of growth of the patches does hemispherical condition next to the surface appear to be limiting.

Appendix II

Equation for calculation of $C^{\frac{1}{2}}$

A. Dissolution Current Density

Assume:

1. Dissolution occurs by Tafel kinetics on bare areas between oxide patches.
2. An ohmic drop between Luggin capillary and specimen surface $\Delta\phi_o = i\rho\bar{\ell}$
3. Uniform macroscopic current density across face of specimen.
4. Avrami condition applies, i.e.,

$$1-\theta = \exp(-\theta_{ex})$$

$$i_+ = i_{o+}\ (1-\theta)\ \exp\left[\frac{\alpha nF}{RT}\ (\phi_p-\phi^e-i\rho\bar{\ell})\right]$$

$$= i_{o+}\ \exp(-\theta_{ex})\ \exp\left[\frac{\alpha nF}{RT}\ (\phi_p-\phi^e-\ i\rho\bar{\ell})\right]$$

$$= i_{o+}\ \exp\left[\frac{\alpha nF}{RT}(\phi_p-\phi^e)\right]\exp\ \left[-\ \frac{\alpha nF\rho\bar{\ell}}{RT}\ i\ -\ \theta_{ex}\right]$$

Taking logarithms, $\ell n\ i_+ = \ell n i_{o+} + \frac{\alpha nF}{RT}\ (\phi_p-\phi^e)\ -\ \frac{\alpha nF\rho\bar{\ell}}{RT}\ i\ -\ \theta_{ex}$

Differentiating, $\frac{d\ell n\bar{i}_+}{d\tau} = -\ \frac{\alpha nF\rho\bar{\ell}}{RT}\ \frac{d\bar{i}}{d\tau} - \frac{d\theta_{ex}}{d\tau}$

B. Equation for Patch Growth

Assume:

1. Instantaneous nucleation of n patches/cm^2
2. Two-dimensional patch growth
3. No thickening of patches until first layer complete.

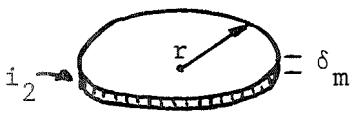

$$d\theta_{ex} = n\,(2\pi r)\,dr$$

$$dr = i_2 \left(\frac{\delta_m}{Q_o}\right) d\tau$$

$$r = \int_0^{\tau} i_2 \left(\frac{\delta_m}{Q_o}\right) d\tau$$

$$d\theta_{ex} = 2\pi n\left(\int_0^{\tau} i_2 \left(\frac{\delta_m}{Q_o}\right) d\tau\right) i_2 \left(\frac{\delta_m}{Q_o}\right) d\tau$$

$$\frac{d\theta_{ex}}{d\tau} = 2C^{\frac{1}{2}} \int_0^{\tau} C^{\frac{1}{2}}\, d\tau$$

where $C^{\frac{1}{2}} = (\pi n)^{\frac{1}{2}} \left(\frac{\delta_m}{Q_o}\right) i_2$

C. Equation to Evaluate $C^{\frac{1}{2}}$

Assume: Current to form patches is negligible compared to current, $\therefore i_+ = i$

Combining final equation in parts A and B

$$\frac{d\ell n i}{d\tau} = -\frac{\alpha n F \rho \bar{\ell}}{RT}\frac{di}{d\tau} - 2C^{\frac{1}{2}}\int_0^{\tau} C^{\frac{1}{2}} d\tau$$

or

$$C^{\frac{1}{2}}\int_0^{\tau} C^{\frac{1}{2}}\, d\tau = -\,{}^{1}/_{2}\left[1 + \left(\frac{\alpha n F \rho \bar{\ell}}{RT}\right) i\right]\frac{d\ell n i}{d\tau}$$

Appendix III

Modified Equation to Calculate Values of $C^{\frac{1}{2}}$

(holes corroded in surface between patches)

Assume: Tangential growth of oxide on surface at velocity ν_o

Normal dissolution rate of metal at velocity ν_+ over the bare surface.

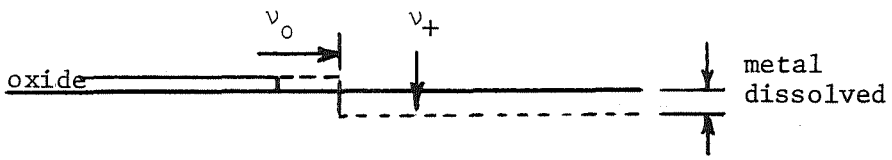

As these two processes continue a contour develops

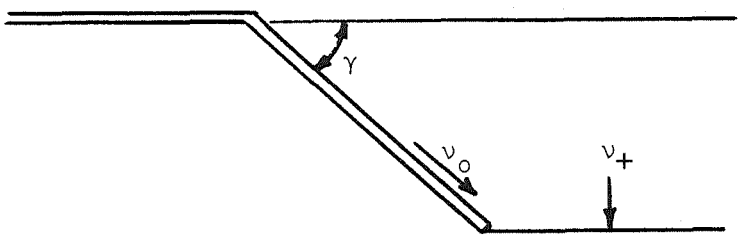

where $\nu_o \sin\gamma = \nu_+$.

Assume n bare areas of initial radius r_o between oxide patches.

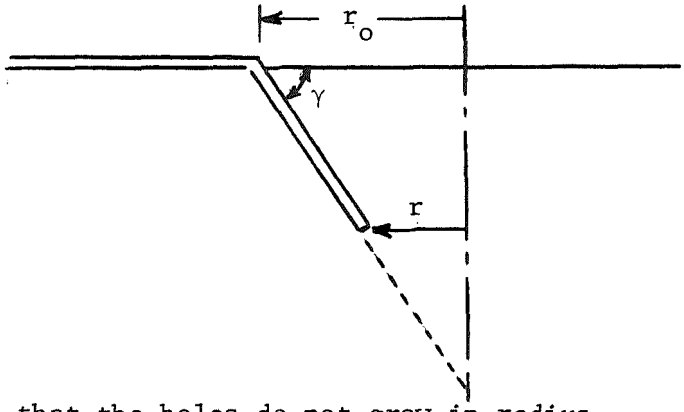

In order that the holes do not grow in radius,

$$\frac{\nu_+}{\nu_o} = \sin\gamma < 1 \; ; \qquad \therefore 0 < \frac{\nu_+}{\nu_o} < 1 \; .$$

If $\nu_+/\nu_o > 1$ the edges of the holes become "undermined." This may be the condition at the pitting potential: i.e., the pitting potential may be determined by kinetics rather than by the thermodynamic considerations suggested by Vetter[29].

$$\nu_o = i_2 \left(\frac{\delta_m}{Q_o}\right)$$

$$\nu_+ = i_+ \left(\frac{M}{zF\rho_d}\right)$$

$$\frac{\nu_+}{\nu_o} = \left(\frac{M \quad Q_o}{zF\rho_d \delta_m}\right) \frac{i_+}{i_2}$$

$$\frac{M\ Q_o}{zF\rho_d \delta_m} \approx 1 \quad \text{for titanium},$$

$$\therefore \frac{\nu_+}{\nu_o} \approx \frac{i_+}{i_2}, \text{ and } 0 < \frac{i_+}{i_2} < 1 .$$

Total current density

$$i = n\ (I_+ + I_o)$$

$$I_+ = \pi r^2 i_+$$

$$I_o = 2\pi r \delta_m i_2$$

For $i_+ \approx i_2$ and $r >> \delta_m$, $I_+ > I_o$

and

$$i \approx n\ I_+$$

$$\approx n \pi r^2 i_+$$

$$dr = -\nu_o \, d\tau \cos\gamma$$

$$= -\left(\frac{\delta m}{Q_o}\right) i_2 \quad d\tau \cos\gamma$$

$$r = r_o - \int_o^\tau dr = r_o - \left(\frac{\delta m}{Q_o}\right)\int_o^\tau i_2 d\tau \cos\gamma$$

$$i \approx n\pi i_+ \left[r_o - \left(\frac{\delta m}{Q_o}\right) \int_o^\tau i_2 \, d\tau \cos\gamma\right]^2$$

$$= i_+ \left[(n\pi)^{\frac{1}{2}} r_o - (n\pi)^{\frac{1}{2}}\left(\frac{\delta m}{Q_o}\right) \int_o^\tau i_2 \, d\tau \cos\gamma \right]^2$$

Let $n\pi r_o^{\,2} = 1$

and $(n\pi)^{\frac{1}{2}} \left(\frac{\delta m}{Q_o}\right) \quad i_2 \quad = C^{\frac{1}{2}}$

$$\therefore i \approx i_+ \left[1 - \cos\gamma \int_o^\tau C^{\frac{1}{2}} \, d\tau\right]^2$$

Using Tafel relation for i_+,

$$i \approx i_o \quad \exp \left[\frac{\alpha n F}{RT} (\phi_p - \phi^e - i\rho \, \bar{\ell})\right]\left[1 - \cos\gamma \int_o^\tau C^{\frac{1}{2}} \quad d\tau \right]^2$$

Taking logarithms,

$$\ell n i = \ell n\ i_o + \frac{\alpha n F}{RT}(\phi_p - \phi^e - i\rho\bar{\ell}) + 2\ell n \left[1 - \cos\gamma \int_0^\tau C^{\frac{1}{2}} d\tau\right]$$

Differentiating,

$$\frac{d\ell n i}{d\tau} = -\frac{\alpha n F \rho \bar{\ell}}{RT} \frac{di}{d\tau} + 2 \frac{d\ell n\left[1 - \cos\gamma \int_0^\tau C^{\frac{1}{2}} d\tau\right]}{d\tau}$$

or

$$1/2 \left[1 + \left(\frac{\alpha n F\ \rho\bar{\ell}}{RT}\ i\right]\right. \frac{d\ell n i}{d\tau} = \frac{d\ell n\left[1 - \cos\gamma \int_0^\tau C^{\frac{1}{2}} d\tau\right]}{d\tau}$$

Appendix IV

Theory for slope of log $C^{\frac{1}{2}}$ vs ϕ

Assume reaction scheme

$$Ti + H_2O \xrightarrow{i_1} TiO + 2H^+ + 2e$$

$$TiO + H_2O \xrightarrow{i_2} TiO_2 + 2H^+ + 2e$$

$$TiO + 2H^+ \xrightarrow{i_3} Ti^{3+} + H_2O + e$$

at steady state,

$$j_1 = j_2 + j_3 \ , \ i = zFj, \therefore \frac{i_1}{2} = \frac{i_2}{2} + i_3$$

Assume Tafel kinetics for reactions 1, 2 and 3 and first order kinetics for reactants

$$i_1 = i_{01} \left(\frac{\alpha_{H_2O}}{\alpha^\circ_{H_2O}}\right) \exp\left[\frac{\alpha_1 n_1 F}{RT} (\phi - \phi_1^e)\right]$$

$$i_2 = i_{02} \left(\frac{\alpha_{TiO}\alpha_{H_2O}}{\alpha^\circ_{TiO}\alpha^\circ_{H_2O}}\right) \exp\left[\frac{\alpha_2 n_2 F}{RT} (\phi - \phi_2^e)\right]$$

$$i_3 = i_{03} \left(\frac{\alpha_{TiO}\alpha_{H^+}}{\alpha^\circ_{TiO}\ \alpha^\circ_{H^+}}\right) \exp\left[\frac{\alpha_3 n_3 F}{RT} (\phi - \phi_3^e)\right]$$

Assume:

1. All reactions referred to mixed potential and

   $\phi_{mi} > \phi_{oi}$, $\eta_m = \phi - \phi_m$

2. α_{H_2O} = constant, α_{H^+} = constant

3. $\Phi = \frac{F}{RT}\phi$, $H = \frac{F}{RT}\eta$

Therefore:

$$i_1 = i_{m1} \exp[\alpha_1 \eta_1 H]$$

$$i_2 = i_{m2} \left(\frac{\alpha_{TiO}}{\alpha^\circ_{TiO}}\right) \exp[\alpha_2 \eta_2 H]$$

$$i_3 = i_{m3} \left(\frac{\alpha_{TiO}}{\alpha^\circ_{TiO}}\right) \exp[\alpha_3 \eta_3 H]$$

Case I: $i_3 >> i_2$, $\therefore i_1 \approx 2i_3$ and

$$i_{mi} \exp[\alpha_1 \eta_1 H] = 2i_{m3} \left(\frac{\alpha_{TiO}}{\alpha^\circ_{TiO}}\right) \exp[\alpha_3 \eta_3 H]$$

$$\left(\frac{\alpha_{TiO}}{\alpha^\circ_{TiO}}\right) = \frac{i_2}{i_{m2} \exp[\alpha_2 \eta_2 H]}$$

$$\therefore i_{mi} \exp[\alpha_1 \eta_1 H] = 2\, i_{m3} \left\{\frac{i_2}{i_{m2} \exp[\alpha_2 \eta_2 H]}\right\} \exp\,[\alpha_3 \eta_3 H]$$

$$i_2 = \frac{i_{m1}\ \exp[\alpha_1\eta_1 H]\ i_{m2}\exp[\alpha_2\eta_2 H]}{2\ i_{m3}\exp[\alpha_3\eta_3 H]}$$

$$= \frac{i_{m1}i_{m2}}{2\ i_{m3}}\ \exp[(\alpha_1\eta_1+\alpha_2\eta_1 - \alpha_3\eta_3)H]$$

$$\ell n i_2 = \ell n\left(\frac{i_{m1}i_{m2}}{2i_{m3}}\right) + (\alpha_1\eta_1 + \alpha_2\eta_2 - \alpha^3\eta_3)H$$

$$\frac{d\ell n i_2}{dH} = (\alpha_1\eta_1 + \alpha_2\eta_2 - \alpha_3\eta_3)$$

$$\frac{d\ \log\ i_2}{d\eta} = \frac{(\alpha_1\eta_1 + \alpha_2\eta_2 - \alpha_3\eta_3)}{2.3\ \ RT/F}$$

$$\frac{d\eta}{d\ \log\ i_2} = \frac{2.3\ RT/F}{(\alpha_1\eta_1 + \alpha_2\eta_2 - \alpha_3\eta_3)} = \frac{59}{(\alpha_1\eta_1 + \alpha_2\eta_2 - \alpha_3\eta_3)}$$

(2.3 RT/F = 59 mv/decade)

Value calculated from experiments = -220 mv/decade

$$(\alpha_1\eta_1 + \alpha_2\eta_2 - \alpha_3\ \eta_3) = \frac{59}{-220} = -\ 0.27$$

Problems:

1. It is not likely that $\alpha_1\eta_1+\alpha_2\eta_2 - \alpha_3\eta_3$ would be negative if $\alpha\eta$'s are all about 1/2.

2. The assumption that $i_3 >> i_2$ is inconsistent with the assumption that $0 < \frac{i_+}{i_2} < 1$ made in Appendix III.

Case II: $i_3 << i_2$

$$\left(\frac{\alpha TiO}{\alpha^\circ TiO}\right) = \frac{i_3}{i_{m3}\ \exp[\alpha_3\eta_3 H]}$$

and

$$i_2 = i_{m2} \left\{\frac{i_3}{i_{m3}\exp[\alpha_3\eta_3\ H]}\right\} \exp[\alpha_2\eta_2 H]$$

$$= i_3 \left(\frac{i_{m2}}{i_{m3}}\right) \exp[(\alpha_2\eta_3 - \alpha_3\eta_3)H]$$

If i_3 is limited such as by mass transport

$$i_2 \propto \exp[(\alpha_2\eta_2 - \alpha_3\eta_3)H]$$

Case II has the virtues that:

1. $\alpha_2\eta_2 - \alpha_3\eta_3$ could be negative.
2. $i_3 << i_2$ is consistent with the assumption that $0 < \frac{i_+}{i_2} < 1$ made in Appendix III.
3. A mass transport limit for Ti^{3+} away from the electrode is consistent with the high anodic current densities at the mixed potential (see below)*.
4. Below the mixed potential (coincidently simultaneous with the mass transport limit for Ti^{3+}) i_2 and therefore $C^{\frac{1}{2}}$ could increase with potential.

---

*Note: At steady state, limiting current density is $i_L = zFD \frac{C_{sat}}{\delta}$.

For $z = 3$

$F \approx 10^5$ coul/mole

$D \approx 10^{-5}$ cm^2/sec

$C_{sat} = 10^{-2}$ $mole/cm^3$

$\delta = 10^{-2}$ cm

$i_L \approx 3$ amp/cm^2.

For one-dimensional unsteady-state diffusion into semi-infinite medium

$$i_L = zFC_{sat}\sqrt{\frac{D}{\pi\tau}}$$

For above values,

τ(sec)	i_L (amp/cm^2)
10^{-4}	500
10^{-2}	50
1	5